Hydraulic controls of summer Arctic pack ice albedo

H. Eicken,[1] T. C. Grenfell,[2] D. K. Perovich,[3] J. A. Richter-Menge,[3] and K. Frey[1,4]

Received 31 May 2003; revised 27 April 2004; accepted 3 June 2004; published 10 August 2004.

[1] Linkages between albedo, surface morphology, melt pond distribution, and properties of first-year and multiyear sea ice have been studied at two field sites in the North American Arctic between 1998 and 2001. It is shown that summer sea-ice albedo depends critically on surface melt-pond hydrology, controlled by melt rate, ice permeability, and topography. Remarkable short-term and interannual variability in pond fraction varying by more than a factor of 2 and hence area-averaged albedo (varying between 0.28 and 0.49 over the period of a few days) were observed to be forced by millimeter to centimeter changes in pond water level. Tracer studies show that the depth of the snow cover, by controlling the amount of superimposed ice formation in early summer, critically affects the retention of meltwater at the ice surface and hence affects pond coverage. Ice roughness as determined by deformation and aging processes explains a significant portion of the contrasts in pond coverage and albedo between ice of different ages, suggesting that a reduction in multiyear ice area and sea-ice residence time in the Arctic Ocean is accompanied by large-scale ice albedo decreases. Our work indicates that ice-albedo prediction in large-scale models with conventional methods is inherently difficult, if not impossible. However, a hydrological model, incorporating measured statistics of ice topography, reproduces observed pond features and variability, pointing toward an alternative approach in predicting ice albedo in numerical simulations. *INDEX TERMS:* 4540 Oceanography: Physical: Ice mechanics and air/sea/ice exchange processes; 1863 Hydrology: Snow and ice (1827); 5114 Physical Properties of Rocks: Permeability and porosity; 1827 Hydrology: Glaciology (1863); *KEYWORDS:* sea ice, albedo, permeability

Citation: Eicken, H., T. C. Grenfell, D. K. Perovich, J. A. Richter-Menge, and K. Frey (2004), Hydraulic controls of summer Arctic pack ice albedo, *J. Geophys. Res.*, *109*, C08007, doi:10.1029/2003JC001989.

1. Introduction

[2] It is generally accepted that feedback processes involving the input of solar energy and subsequent changes in Arctic pack-ice albedo are a key aspect of the polar amplification of climate variability and change [*Untersteiner*, 1990; *Schramm et al.*, 1997; *Perovich et al.*, 1999; *Folland et al.*, 2001]. Recent efforts have focused on the detection of signals of climate change in the Arctic [*Serreze et al.*, 2000; *Folland et al.*, 2001] as well as improvement of sea-ice dynamics in global circulation models (GCMs) [*Lemke et al.*, 1997]. The summer heat budget of Arctic sea ice has received less attention [*Perovich et al.*, 1999; *Walsh et al.*, 2001], generally justified by the adequate performance of even simple sea ice models in reproducing the annual cycle of ice mass balance [*Untersteiner*, 1990; *Steele and Flato*, 2000]. Ironically, the strong dependence of the pack-ice mass balance on albedo may be indirectly responsible for reasonable correspondence between models and measurements. Even minor changes in the magnitude of summer ice albedo have a strong impact on ice extent and volume. Hence albedo is commonly used as a "model tuning parameter" [*Maykut*, 1986; *Curry et al.*, 2001]. In a recent study, comparing large-scale model simulations and measurements, *Rothrock et al.* [2003] identified the strong impact of "radiative formulations and treatment of ice albedo" on mean thickness as a key factor in explaining deviations between individual models and ice-thickness data sets.

[3] In summer, the Arctic Ocean surface consists of a mixture of open water, bare white ice, and ice covered with melt ponds. A recent evaluation identified the need for surface albedo measurements including data on the pond coverage second only to precipitation on a list of 10 high-priority polar measurements [*Walsh et al.*, 2001]. Of the three surface types, the albedo of open water and bare first-year and multiyear ice are remarkably stable at 0.07, 0.60, and 0.65, respectively [*Grenfell and Perovich*, 1984; *Pegau and Paulson*, 2001; *Perovich et al.*, 2002b]. The albedo of ponded ice is more variable, typically ranging from 0.2 to 0.4 [*Perovich et al.*, 2002b]. Melt ponds mostly cover between 10 and 50% of the ice surface [*Romanov*, 1995; *Tschudi et al.*, 2001; *Perovich et al.*, 2002a], and their areal fraction controls the integrated ice surface albedo, as dem-

[1]Geophysical Institute, University of Alaska Fairbanks, Fairbanks, Alaska, USA.
[2]Department of Atmospheric Sciences, University of Washington, Seattle, Washington, USA.
[3]Cold Regions Research and Engineering Laboratory, Hanover, New Hampshire, USA.
[4]Deceased 24 March 2002.

0148-0227/04/2003JC001989$09.00

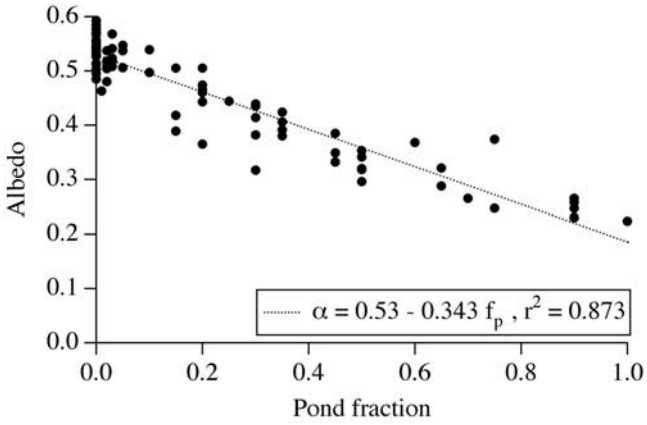

Figure 1. Albedo α as a function of pond areal fraction f_p, estimated visually within the instrument footprint as measured in first-year sea ice at Barrow on 4 June 2001 along a 200-m profile. Note the linear dependence of albedo on the fraction of bare ice and ponds (linear least squares regression fit is indicated in the figure legend).

onstrated by the albedo measurements shown in Figure 1. With ice concentrations >85% in the interior Arctic, the spatial and temporal variability of ponded ice albedo is hence a key parameter in determining the large-scale sea-ice albedo and its importance for the hemispheric radiation balance. While models perform adequately at estimating the distribution of ice and open water, we are not aware of models capable of predicting pond fractions. Despite advances in modeling summer ice albedo evolution [*Schramm et al.*, 1997; *Curry et al.*, 2001], even the most sophisticated of these models currently assume an ad hoc pond fraction and hence assume ice albedo. Here we assess the dependence of ice-albedo evolution on sea-ice and meltwater processes based on field measurements in first-year and multiyear Arctic sea ice, identify problems in simulating the seasonal cycle of ice albedo, and discuss a possible alternative approach to the problem.

2. Methods

[4] A summer ice optics, mass balance, and hydrological research program was carried out in 1998 at the Surface Heat Budget of the Arctic Ocean (SHEBA) Study Site in multiyear ice of the northern Chukchi Sea [*Perovich et al.*, 1999; *Eicken et al.*, 2002] and in 2000 and 2001 in first-year landfast ice off Barrow in northern Alaska (Figure 2).

[5] Every 1 to 4 days a series of measurements was carried out along 200-m profiles representative of the different ice types ($\leq$1-m intervals). The profiles were marked with stakes placed at approximately 50-m intervals in the upper layers of the ice cover, with distances in between stakes determined by tape measure. In order to minimize disturbance of the ice surface and avoid artificial modification of the ponding and the surface albedo, the measurement plots beyond the stakes were off-limits and not stepped on during the entire duration of the experiment. Traffic on the proximal side of the profile was limited to a single visit on foot every 1 to 4 days, and care was taken so as not to disturb the ice surface or the melt ponds. No samples or holes were drilled within the drainage area of ponds crossing the measurement line. With these precautions, the amount of site disturbance was kept to an absolute minimum and did not result in any measurement bias or artifact.

[6] At the SHEBA site, measurements were carried out along profiles in level ice with ancillary measurements of topography and melt ponding also in deformed ice. At Barrow, the profiles were confined to level ice with small-scale, natural roughness features. Measurements along the profiles included snow depth, melt pond depth, and surface topography relative to sea level with a laser surveying apparatus with a precision of better than 10 mm [*Eicken et al.*, 2001]. Total and spectral albedo were measured every 2.5 m along the same profiles with a Kipp and Zonen albedometer and one of two diode array spectrophotometers [*Perovich et al.*, 2002b]. During SHEBA a Spectron Engineering SE590 was used with three separate camera heads providing wavelength coverage from 320 to about 1500 nm. At Barrow an ASD Fieldspec Pro was introduced, increasing the wavelength range from 320 to 2500 nm. The spectrophotometers were fitted with wide-band cosine receptors so that the instrument output was directly proportional to irradiance to provide accurate albedo results (to within about 2%) under both clear-sky and overcast conditions.

[7] Ice physical properties were measured on 10-cm-diameter core samples. Ice cores were photographed for pore textural analysis and cut into 5- to 10-cm subsections within minutes after sampling. These core segments were transferred to the lab and melted for measurements of salinity with a YSI 30 conductivity probe (measurement

Figure 2. Map showing Barrow sampling site and drift of SHEBA ice camp between 1 June and 30 August 1998 (moving from south to north). Thick line indicates position of ice edge on 2 September 1998 according to U.S. National Ice Center charts.

error <0.02 or <1% of the bulk salinity, whichever is larger). Stable-isotope samples were transferred to glass vials for subsequent measurements in Fairbanks. At selected locations, thick and thin section samples were also cut. Temperature profiles at 5 to 10 cm spacing have also been obtained at 10-min intervals from a series of thermistor strings frozen into the ice in the previous fall. The instrument setup and details of the measurements are described by *Frey et al.* [2001]. Measurements from in situ probes were supplemented by direct measurements taken with a thermistor probe inserted into holes drilled to the center of a second ice core taken at the measurement site (accuracy better than 0.2 K). In situ brine volumes were derived from the ice salinity and temperature measurements as described by *Cox and Weeks* [1983] and *Leppäranta and Manninen* [1988]. Bottom and surface ice ablation were measured in the immediate vicinity of these sites in the northern Chukchi Sea and near Barrow with heated-wire mass balance gauges frozen into the ice at the start of winter as described by *Perovich et al.* [2003].

[8] Ice permeability and meltwater diversion were studied with the aid of fluorescent and stable-isotope tracers ($\delta^{18}O$) and through borehole bail tests [*Eicken et al.*, 2002; *Freitag and Eicken*, 2003]. In brief, known amounts of the tracer, typically between 250 and 1000 mg of either Fluoresceine (FLC) or Sulforhodamine B (SRB) were released into 5-cm-diameter boreholes or melt ponds after deployment of an array of samplers to monitor dispersion of the tracer as a function of time. In monitoring flow through networks of connected melt ponds with low meltwater residence times, the tracer front was also tracked visually. Concentrations were measured with a Shimadzu RF1501 spectrofluorometer, buffering the sample to a pH of 8.0, at excitation and emission wavelengths of 491 and 512 nm for FLC and 564 and 583 nm for SRB. Calibration was carried out at the start and end of the field campaign against a dilution series of fresh stock solutions.

[9] The borehole bail tests consisted of drilling a 14-cm-diameter hole to a given depth level in the ice, inserting a packer (metal tube with an inflatable outer rubber jacket, pressing against the hole wall) that limits the influx of water and brine in the hole to that passing through its bottom surface. An ultrasonic transducer measured the water level in the hole as a function of time, $h(t)$. The permeability in the vertical direction k_z can then be derived by integrating

$$h(t) = h(t_0)\exp\left(-k_z \frac{g\rho}{\mu L} t\right), \quad (1)$$

with gravitational acceleration g, fluid density ρ, and dynamic viscosity μ; L is the thickness of the underlying ice layer, and $h(t_0)$ is the water level at the start of the experiment. A correction based on two-dimensional flow modeling has to be applied to account for flow into the hole from directions other than z [*Freitag and Eicken*, 2003]. Absolute errors in measurements of permeability amount to less than 50%.

[10] Stable-isotope data of ice and pond-water samples were measured at the analytical facilities of the Frontier Research Program/International Arctic Research Center at the University of Alaska Fairbanks on a Finnigan MAT 252 mass spectrometer. Samples were equilibrated with CO_2, with measurements calibrated against Vienna Standard Mean Ocean Water (VSMOW) and Standard Light Antarctic Precipitation (SLAP) standards. Standard errors as determined for eight laboratory standards measured within a batch of 40 samples typically range between 0.02 and 0.03‰ (in $\delta^{18}O$ notation).

[11] Surface-based observations at Barrow were complemented by aerial digital photography obtained with a vertically downward looking camera (ground-projected pixel size <1 m) flown every 1 to 3 days during the earlier stages of the melt season at altitudes of 300 to 1500 m. At SHEBA, aerial photography was obtained mostly at 2000 m altitude with some low-level flights down to 300 m. While the ice studied at SHEBA appears representative of perennial Arctic sea ice [*Perovich et al.*, 1999], the setting at Barrow results in a landfast-ice cover that is typical of first-year drifting pack ice, rather than the smooth fast ice devoid of deformation features [*Shapiro and Barnes*, 1991].

3. Results From Field Measurements

3.1. Control of Pond Area: Permeability, Net Meltwater Production, and Topography

[12] The field measurements were aimed at elucidating the linkages between meltwater production, surface topography, and ice albedo (Figures 3, 4, and 5and Table 1). The data from level multiyear ice at the SHEBA camp demonstrate a gradual decline in pond fraction f_p from 0.46 to 0.30 during the first half of the melt season (Figure 3). On the basis of criteria detailed by *Eicken et al.* [2002], the first half of the melt season for first-year ice at Barrow extends from approximately 25 May to 20 June, while ranging from 29 May to 9 July on multiyear sea ice at SHEBA. The decrease in pond fraction corresponds to a steady drop in pond hydraulic head, i.e., the elevation of water surfaces corrected for differences in fluid potential [*Eicken et al.*, 2002; *Perovich et al.*, 2002b]. While aerial surveys of pond fractions show overall lower numbers due to the inclusion of other ice classes with fewer ponds [*Perovich et al.*, 2002a, 2002b], the overall seasonal trend was the same as along the individual profiles. Thus, as long as appreciable hydraulic gradients persisted prior to about 9 July at the SHEBA site, pond water was redistributed across the surface over distances of tens to hundreds of meters, guided by the topography (Figure 4) [*Eicken et al.*, 2002; *Freitag and Eicken*, 2003]. At the same time, pond water drained through the porous ice matrix and flaws or cracks. The same evolution, though with more substantial short-term and interannual variability, has been observed in first-year ice near Barrow, Alaska.

[13] The measurements of surface topography and pond hydrology demonstrate that pond area and hence albedo [*Curry et al.*, 1995; *Fetterer and Untersteiner*, 1998; *Eicken et al.*, 2002] are forced by differences in hydraulic head or elevation of at most <200 mm for multiyear and <140 mm for first-year ice (Figure 3). This holds true both for short timescales such as the diurnal variations in pond-water level recorded by pressure transducer over first-year ice (Figure 3, solid lines) and for the longer-term seasonal evolution with pond water surfaces approaching equilibrium level during the course of June with concurrent shrinking of ponds (Figure 3, blue asterisks). Decreasing pond hydraulic head toward the second half of the melt season greatly reduces lateral melt-

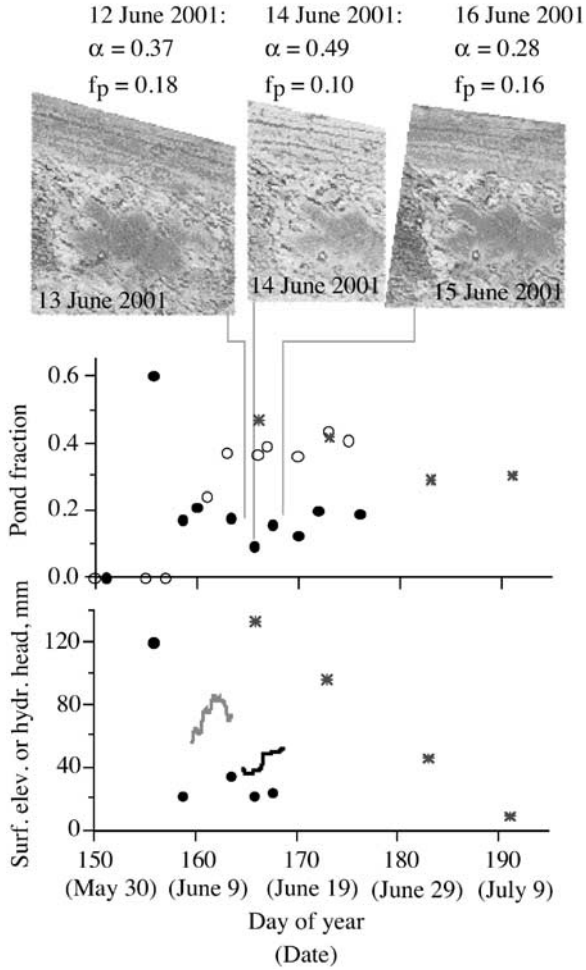

Figure 3. Areal fraction and hydraulic head of melt ponds in multiyear ice (asterisks, measurements carried out at SHEBA sites along a 100-m profile through level ice) and first-year ice near Barrow (open circles: 2000; dots: 2001). Solid lines show water level in a single pond (pressure-gauge measurement; red: 2000; black: 2001). Aerial photographs (top middle panel, ~600 m wide; dates of overflights indicated at bottom of photograph) show a sequence of drainage and flooding events in first-year ice near Barrow. Also shown are areally averaged albedo α and pond fraction f_p (measurement dates are indicated at top; note that on two dates, synchronous overflights and ground-based measurements were not possible). See color version of this figure at back of this issue.

water transport, reducing shrinkage or expansion of ponds in combination with steepening of ponds walls.

[14] Even more striking are short-term changes in pond water level and area-averaged ice albedo. At Barrow, a decrease in surface meltwater production between 12 and 16 June (4.2 mm d^{-1} maximum) induced a drop in water level of 4–13 mm (Figure 3) with albedo, α, increasing from 0.37 to 0.49. This was followed by an increase in surface melt driving water levels up by 3–14 mm with α dropping to 0.28. Pond water level represents the balance between downward percolation, surface topography, and meltwater production, i.e., surface ablation rate dH_s/dt (Figure 4), with H_s the height of the ice surface relative to a fixed horizon in the ice interior. With ice permeability and topography varying on timescales of days to weeks and dH_s/dt varying on timescales of hours, reductions in surface ablation during colder periods precipitate rapid shrinkage of pond area (f_p) by a factor of 0.6 or more, with subsequent increase by 1.6 due to an increase in dH_s/dt, corresponding to measured changes in albedo by factors of 1.3 and 1.8. This variability in albedo due to variations in pond areal extent and meltwater saturation of pond margins is controlled by millimeter- to centimeter-scale water level variations. During the latter part of the melt season in multiyear ice (not shown in Figure 3), pond areal extent increases again due to infiltration of pond margins and lateral melt. At this point, however, the pond hydraulic head in level ice is not sufficient to drive significant flow, and other processes control widening of ponds [*Eicken et al.*, 2002].

[15] The sensitivity to pond-level variations is more pronounced in the smoother first-year as compared to multiyear ice. While this is partially evident from Figure 3, we have examined the role of surface topography in more detail by comparing surface elevation profiles and pond fractions for three different ice types: level first-year sea ice at Barrow (Figure 5a) and level and rough multiyear sea ice at SHEBA (Figures 5b and 5c). These data, summarized in Table 1, demonstrate that the comparatively smooth first-year ice (with the standard deviation of ice surface elevation as a measure of roughness (Figure 5a)) exhibits the broadest range of pond fractions. Typically, pond fractions on first-year ice are higher than the mean value of 0.19 shown here, ranging more toward the maximum observed value of 0.60 [*Derksen et al.*, 1997; *Hanesiak et al.*, 2001]. The causes for the comparatively low values measured in 2001, also in comparison with measurements made in 2000 (Table 2) are examined in more detail below. Level multiyear ice, while somewhat rougher as a result of deepening of ponds during subsequent melt periods [*Eicken et al.*, 2001], still exhibits a substantial range in pond fractions, though not as large as that in smoother first-year ice. Finally, the smallest range in pond fractions and the overall lowest mean pond fractions were observed in rough multiyear ice, with a surface characterized by both deformation features and deepened melt pools (Figure 5c).

[16] Aerial photographs and on-ice observations corroborate the topographically controlled waxing and waning of ponds (Figure 3). In contrast with other factors driving

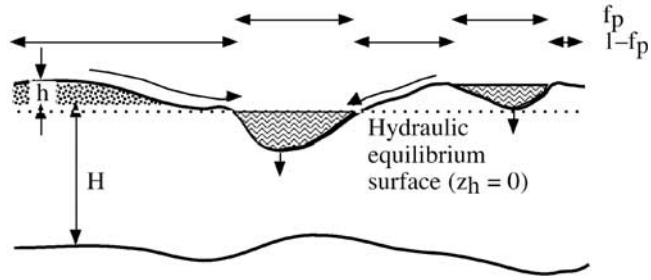

Figure 4. Schematic diagram showing fractions of ponds f_p and ice of thickness H with and without snow cover of depth h. Pathways of meltwater flow (single arrows) are also shown.

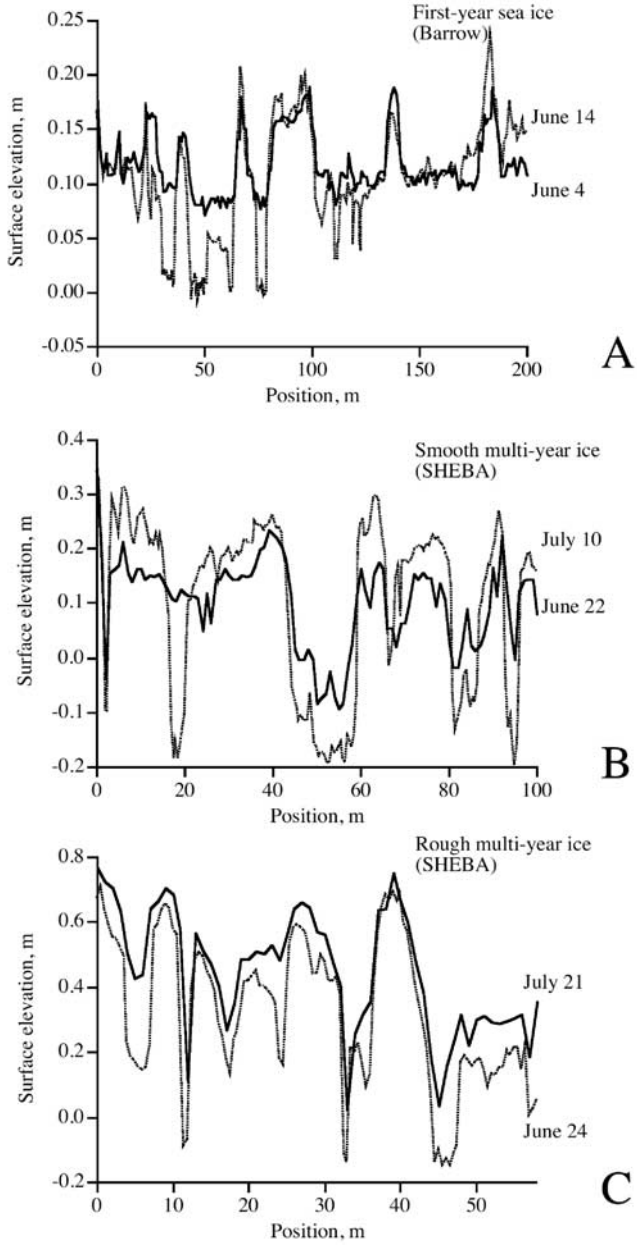

Figure 5. Surface topography profiles in different ice types in early and midmelt season. (a) Level first-year sea ice at Barrow, Alaska (the corresponding albedo measurements along this profile are shown in Figure 1). (b) Level multiyear sea ice at the SHEBA site. (c) Rough multiyear sea ice at the SHEBA site. Mean surface elevation and pond fraction are indicated in Table 1 for all three ice types.

albedo changes, such hydraulically forced variations are near instantaneous. Diurnal changes in meltwater production result in substantial differences in pond water level (Figure 3) and hence pond areal extent [*Perovich et al.*, 2002b; *Eicken et al.*, 2002]. This variability is of importance, for example, for sea-ice remote sensing [*Robinson et al.*, 1992; *El Naggar et al.*, 1998; *Yackel and Barber*, 2000] or travel on ice (locals favor the "dry" early morning hours for travel over ice [*Parry*, 1828; R. Glenn, personal communication, 2001]). Potentially most important are the ramifications for short- and long-term variations in albedo, however. The common strategy of centering albedo measurements around solar noon [*Perovich et al.*, 2002b], i.e., when meltwater production rates and hence pond coverage are about to peak (Figure 3), may result in a substantial bias transferred into model parameterizations, at least during the first part of the melt season when pond water levels are far from hydrostatic equilibrium.

Table 1. Mean and Standard Deviation of Surface Elevation and Mean, Minimum, and Maximum Areal Pond Fractions Along Fixed Profiles in Different Ice Types[a]

Dates	z_{sc}, m ($\pm\sigma$)	f_p ($\pm\sigma$)	Min(f_p)	Max(f_p)
Level First-Year Ice (Barrow)				
4 June 2001	0.12 ± 0.03	0.60		
14 June 2001	0.08 ± 0.06	0.18		
Mean (entire melt season)		0.19 ± 0.16	0.10	0.60
Level Multiyear Ice (SHEBA)				
22 June 1998	0.10 ± 0.08	0.42		
10 July 1998	0.10 ± 0.16	0.30		
Mean (entire melt season)		0.32 ± 0.16	0.29	0.46
Rough Multiyear Ice (SHEBA)				
24 June 1998	0.45 ± 0.19	0.15		
21 July 1998	0.32 ± 0.23	0. 09		
Mean (entire melt season)		0.13 ± 0.07	0.09	0.21

[a]Surface elevation measurements include the bottom of ponds.

3.2. Role of Snow Cover and Superimposed Ice Formation

[17] The differences between pond fractions in level and deformed multiyear ice at SHEBA (f_p = 0.32 or 0.13, Table 1) are due to differences in surface topography [*Eicken et al.*, 2001, 2002]. However, topography does not explain the contrast between the 2000 and 2001 Barrow data (f_p = 0.39 and 0.17 respectively, or, including the snow covered part of the season, f_p = 0.26, 0.19, Table 2), since the ice was rougher in 2000 than in 2001, suggesting a trend in the opposite direction if topography alone were controlling these interannual changes. The impact of permeability variations also needs to be taken into account. To do this, the vertical permeability structure of the ice was derived from a porosity-permeability model. On the basis of a series of measurements of ice permeability over the entire ice thickness throughout the ice season in 1998/1999 and 1999/2000 (H. Eicken et al., Permeability-porosity relationships in first-year Arctic sea ice, manuscript in preparation, 2004) (hereinafter referred to as Eicken et al., manuscript in

Table 2. Contrasts in Albedo, Meltpond Fraction, and Ice Permeability[a]

Ice Type, Dates	α	f_p	h, m	f_{si}	k_t, 10^{-11} m^2
Multiyear ice, 27 May to 12 August 1998	0.53	0.32	0.34	0.38	48
First-year ice, 29 May to 28 June 2000	0.45	0.26	0.24	0.50	2.4
First-year ice, 27 May to 25 June 2001	0.50	0.19	0.10	0.05	12

[a]Mean albedo α, pond fraction f_p, maximum snow depth h, fraction of meteoric superimposed ice f_{si} (in uppermost 0.10 m on 1 June 1998 and 7 June 2000 and 2001), and permeability k_t of the uppermost one third of the ice cover (based on measurements at SHEBA and derived from porosity-permeability multilayer model at Barrow).

preparation, 2004), a relation between the brine volume fraction V_b and the intrinsic permeability k has been derived (correlation coefficient r for regression is also indicated),

$$k = 4.708 \times 10^{-14} \exp(0.07690\, V_b)\ \mathrm{m}^2 \quad V_b \le 96\,‰ \quad r = 0.74$$

$$k = 3.738 \times 10^{-11} \exp(0.007265\, V_b)\ \mathrm{m}^2 \quad V_b > 96\,‰ \quad r = 0.32. \tag{2}$$

[18] The brine volume fraction has been determined from thermodynamic phase relations as described by *Cox and Weeks* [1983] and *Leppäranta and Manninen* [1988], based on ice core salinity measurements and temperature profiles obtained from thermistor arrays frozen into the ice (profiles obtained at 0200 local solar time were employed to remove bias due to potential solar heating of sensor). Figure 6 shows the permeability profile derived from these calculations for the ice cover during the early melt season on 9 June in 2000 and 2001. The largest differences in permeability were found in the uppermost ice layers, with the two values from the upper 0.1 m more than 1 order of magnitude smaller in 2000 as compared to 2001. At greater depths, differences in permeability are less significant. Assuming that the permeability structure of the ice is controlled by the vertical layering of temperature and salinity, which in turn control brine volume fractions, and that permeabilities in the vertical z-direction are more than an order of magnitude larger than those in the horizontal [*Freitag*, 1999; Eicken et al., manuscript in preparation, 2004], the bulk ice permeability k can be derived from the harmonic mean of the vertical permeability profile, constituted of n layers of permeability k_i,

$$k = n\left[\sum_i \left(\frac{1}{k_i}\right)\right]^{-1}. \tag{3}$$

In this case, it is the low surface permeabilities that appear to be responsible for the contrasts in meltwater retention

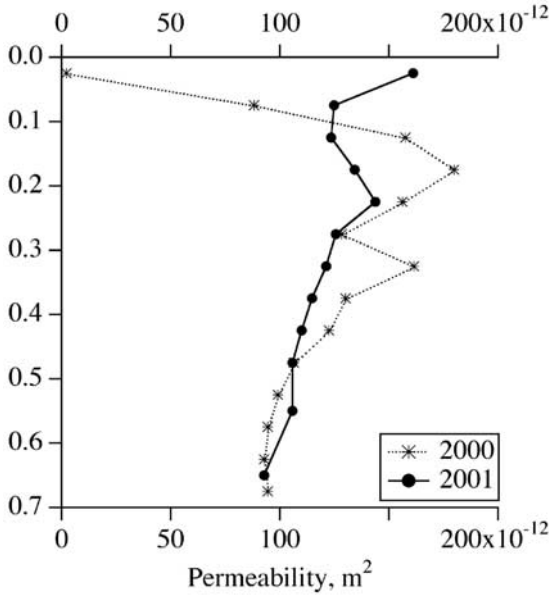

Figure 6. Permeability profile through the uppermost layers of the ice cover as derived from ice core temperature and salinity measurements and a porosity-permeability model for 9 June 2000 and 2001.

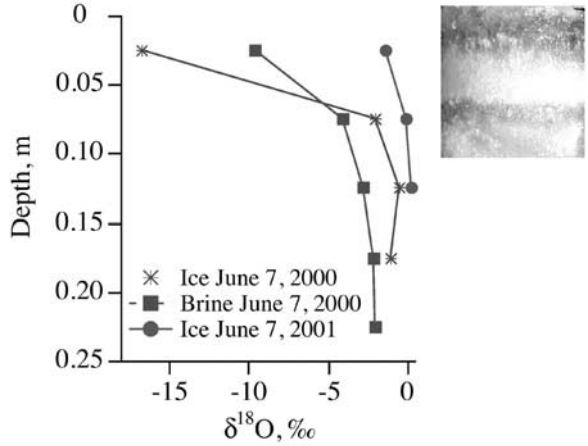

Figure 7. Stable-isotope profiles of the uppermost ice layers for cores collected on 7 June in 2000 and 2001. Asterisks and dots show measurements on solid ice samples, and squares correspond to data obtained on brine removed from the ice through centrifugation. The core stratigraphic photograph at right is for the 2000 core, showing the extent of the low-permeability superimposed ice layer, corresponding to the δ^{18}O minimum at the surface.

between 2000 and 2001 as they control the order-of-magnitude difference in the bulk permeability of the ice (Table 2). In 2000, the ice was overlain by a fresh, low-permeability ice layer that persisted into mid-June and thus effectively sealed the above-freeboard surface layer (Figures 6 and 7). In 2001, this layer developed for 3 days during early melt and was absent for the remainder of the season.

[19] Stable-isotope and stratigraphic core analysis (Figure 7, Table 2) as well as field observations and the temperature profile data indicate that this surface impervious layer formed through freezing of snowmelt water onto the cold ice surface. Formation of superimposed ice during Arctic spring and summer has been observed previously [e.g., *Cherepanov*, 1973], but has been generally considered to be rare, short-lived, and of little importance in the Arctic, as compared to the Antarctic, where thicker snow cover favors superimposed ice formation in areas of perennial ice [e.g., *Haas et al.*, 2001]. In this case, much higher snow depths on first-year ice in 2000 (Table 2), provided a larger freshwater reservoir in the snowpack while at the same time maintaining lower ice surface temperatures due to enhanced thermal insulation. Both of these factors helped maintain an impervious superimposed ice layer composed largely of refrozen snowmelt for a longer period of time compared to 2001 when thin snow cover kept down superimposed ice formation. This interpretation is supported by the stable-isotopic composition of the upper ice layers. On the basis of a simple linear mixing model, the fraction of meteoric superimposed ice f_{si} can be derived from the composition of the bulk sea ice layer δ^{18}O(sample), and pure end-member compositions of sea ice δ^{18}O(sea ice) and snow δ^{18}O(snow),

$$f_{si} = \frac{[\delta^{18}O(\mathrm{sample}) - \delta^{18}O(\mathrm{sea\ ice})]}{[\delta^{18}O(\mathrm{snow}) - \delta^{18}O(\mathrm{sea\ ice})]}. \tag{4}$$

From measurements of end-member compositions (δ^{18}O(sea ice) of −1.8, −0.25, and 0.20 ‰, δ^{18}O(snow) of −23.2, −18.6, or −20.1 ‰ for SHEBA 1998 and Barrow 2000 and 2001, respectively), we determined that 50% of the uppermost 0.1 m was composed of meteoric superimposed ice in 2000, contrasting with 2001 when meteoric superimposed ice only accounted for 5% (Table 2).

[20] Most likely, we are overestimating the permeability of the uppermost superimposed ice layer and underestimating the differences in permeability between 2000 and 2001. Since the permeability-porosity model is based on bulk measurements of the permeability of ordinary congelation ice in the lower half of the ice cover, it does not capture the specific properties of the thin, low-porosity superimposed layer at the very surface. Hence the data presented here can only provide a first indication and further laboratory and field measurements are required to improve estimates of superimposed ice permeability. Further evidence for linkages between snow depth and pond fraction was obtained during SHEBA at the airstrip, where snow was completely removed from first-year ice for maintenance, resulting in pond fractions close to zero compared to much higher pond fractions on undisturbed ice.

4. A Simple Pond Hydrological Model

[21] The sensitivity of pond fraction and area-averaged albedo to even small changes in pond water level presents a formidable challenge for models and albedo parameterization schemes. Model predictions of ice topography at vertical and lateral scales of <10 mm and <1 m appear unrealistic at present. Exploring an alternative approach, we have developed a simple ice hydrological model to assess whether a statistical, rather than an explicit representation of surface topography suffices in predicting pond fractions and hence albedo. Tracer measurements demonstrated that during early melt, lateral meltwater advection rates are several orders of magnitude higher than vertical percolation into the ice [*Eicken et al.*, 2002; *Freitag and Eicken*, 2003] (Figure 4). Hence, in steady state the hydrological balance of melt ponds is given by the surface meltwater production rate ($\rho_i/\rho_{fl} dH_s/dt$) of unponded ice, hydraulic head z_h, and permeability k of the underlying ice, based on the reasonable assumption of Darcian flow [*Freitag*, 1999], (Figure 4),

$$(1 - f_p)\frac{\rho_i}{\rho_{fl}}\frac{dH_s}{dt} = \frac{f_p k \rho_{fl} g}{\eta}\frac{z_h}{H}, \quad (5)$$

with gravitational acceleration g, ice thickness H (1.5 and 2.5 m for first-year and multiyear ice), fluid density ρ_{fl}, ice density ρ_i and kinematic viscosity η. Melting at the pond base is neglected. Tracer studies and pond level measurements [*Eicken et al.*, 2002] indicate that most ponds attain a water level within a narrow range as they are either in hydraulic communication or form as a result of water flowing into topographic depressions. While this may not hold for ponds in ridged areas, the latter typically exhibit low pond coverage with less temporal change and can be disregarded in this context. Thus pond coverage and water level associated with a given set of boundary conditions can be described statistically by determining the cumulative frequency distribution function of ice surface elevation (hypsographic curve). We have obtained such surface elevation data relative to the hydraulic equilibrium surface through surveying with a laser leveling device (Figures 5 and 8). From the probability distribution $p(z)$, we derive f_p,

$$f_p = \int_{z_0}^{z_h} p(z)dz, \quad (6)$$

with minimum ice surface elevation z_0. Equations (5) and (6) were solved numerically for z_h based on time series of surface elevation data $p(z)$. Values of k and ($\rho_i/\rho_{fl} dH_s/dt$) were varied between 10^{-12} and 10^{-9} m^2 and 0.002 and 0.05 m d^{-1}, respectively, in accordance with field measurements (Figure 8) [*Freitag and Eicken*, 2003; *Eicken et al.*, 2002; *Perovich et al.*, 2003; Eicken et al., manuscript in preparation, 2004].

[22] The model indicates good agreement between measurements in multiyear ice and simulated pond fractions and depths, with a typical melt rate of 0.01 m d^{-1} and a permeability of 10^{-12} m^2 (Figures 8a and 8b). The same holds for first-year sea ice (Figures 8c and 8d). The factor of 2 difference in f_p between the 2000 and 2001 data as well as short-term variability (see Figure 3) can be explained by lower permeabilities in 2000 with an impervious surface layer (Figures 6 and 7) and variations in the surface meltwater production rate ranging from above 0.05 m d^{-1} to less than a few mm d^{-1}. Later in the season, the distribution function evolves such that the sensitivity of pond fraction to changes in water level is greatly reduced. This is due to steepening of pond sidewalls as a result of higher melt rates in low-albedo ponds compared to bare white ice. Hence pond and albedo evolution depend strongly on conditions during early melt where such spatial patterns are established. Increasing permeabilities and topographic containment greatly reduce pond area and albedo variability during the later melt season since pond expansion requires lateral infiltration and complete melt rather than simple surface flooding [*Eicken et al.*, 2002]. As permeability increases later in the season, only high melt rates can sustain nonzero pond hydraulic heads in high-permeability multiyear ice (Figure 8b).

5. Discussion

5.1. Pond Evolution, Surface Topography, and Ice-Albedo Feedback

[23] The role of ice-albedo feedback in modulating the Arctic regions' response to variations in surface forcing is well recognized [*Covey et al.*, 1991; *Curry et al.*, 1995; *Fetterer and Untersteiner*, 1998]. Mostly, these feedback processes are considered in terms of a shrinking or expanding ice cover, with resulting contrasts in large-scale albedo due to differences between ice and open water albedos. Research carried out as part of the SHEBA program has also given some consideration to feedback processes confined to the ice cover itself, such as changes in ice albedo due to pond widening and deepening (Figure 1) [see *Perovich et al.*, 2002a, 2002b; *Eicken et al.*, 2002]. Such processes are important in their own right, since the impact of a 10% summer ice-extent anomaly in the Arctic Ocean on shortwave absorption by the ice-ocean system (all other factors remaining the same) would be roughly equivalent to a

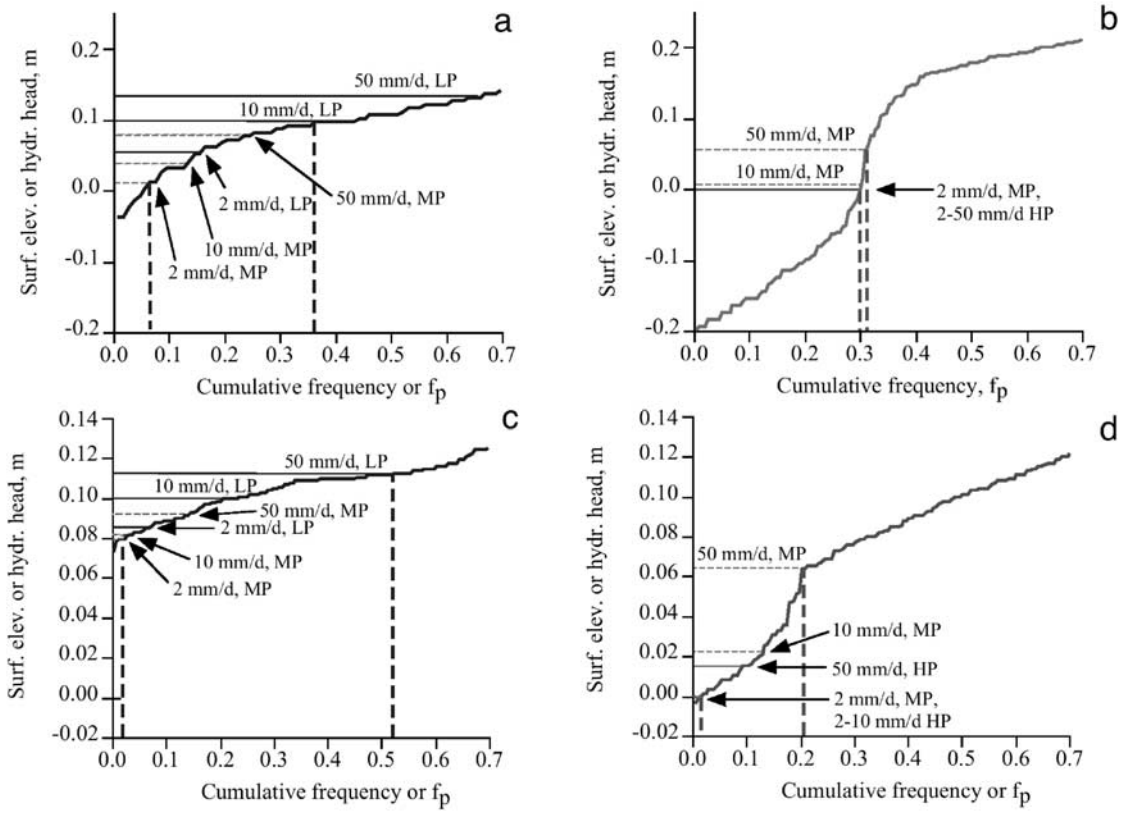

Figure 8. Hypsographic curves and results from pond hydrological model in early and midmelt for multiyear ice on (a) 15 June 1998 and (b) 10 July 1998 and for first-year ice on (c) 4 June 2001 and (d) 14 June 2001. Horizontal lines indicate the steady state pond hydraulic head in level ice as a function of surface ablation rate (lines individually labeled) and ice permeability k (blue: low permeability, LP, 10^{-12} m^2; green: medium permeability, MP, 10^{-11} m^2; red: high permeability, HP, 10^{-10} m^2, during early melt $k \leq 10^{-11}$ m^2 due to the presence of superimposed ice and lower bulk permeabilities; in middle to late melt, $k \geq 10^{-11}$ m^2) as based on in situ measurements [*Eicken et al.*, 2002, 2004]. The range of attainable melt pond coverages, which corresponds to the cumulative frequency interval or f_p marked by the vertical dashed lines, decreases with steepening pond walls, greatly reducing lateral shrinkage, or expansion of ponds during the latter melt season (see also Figure 2).

change in bare-ice albedo by 0.05. This is well within the range of interannual and ice-type dependent albedo variations observed in this study.

[24] The present study demonstrates, however, that changes in summer-ice albedo due to melt pond variations are quite complex and depend on a number of factors whose impacts can either combine or cancel out. This problem is schematically illustrated in Figure 9. Thus, areal pond coverage decreases with age for unridged, "level" sea ice as a result of the deepening of individual ponds due to higher melt rates [*Hanson*, 1965; *Perovich et al.*, 2003]. This process is reflected in the roughening of the topography of both first-year and multiyear ice at Barrow and SHEBA during the course of the melt season (Figures 5 and 8). The hypsographic curves for different types of unridged ice (Figure 8) and the surface elevation profiles (Figure 5) in conjunction with the observed ranges in pond fraction (Table 1) also indicate that pond areal extent is highly sensitive to even small changes in the surface topography. Hence ice deformation and, in particular, ridging have a pronounced impact on pond fractions (see level and deformed ice profiles shown in Figure 5). In ridged areas it is not simply the confinement of surface meltwater into deeper reservoirs between deformation features but also steeper slopes, higher hydraulic heads, and higher permeabilities that help reduce pond fractions compared to level ice, as illustrated by the pond distribution in the vicinity of the prominent ridge shown in Figure 9b and the surface elevation profile shown in Figure 5c with correspondingly low pond fractions (Table 1). Ice deformation is considered a key process in compensating for some of the changes in the surface energy balance resulting in less ice growth [e.g., *Steele and Flato*, 2000]. At the same time, ice deformation can also help reduce the amount of shortwave radiation absorbed by the ice-ocean system due to lowering of melt pond fractions.

[25] However, in assessing the impact of ice surface topography and roughness on pond coverage and albedo, recent observations of increasing fractions of first-year ice in the Arctic Ocean due to a reduction in summer minimum

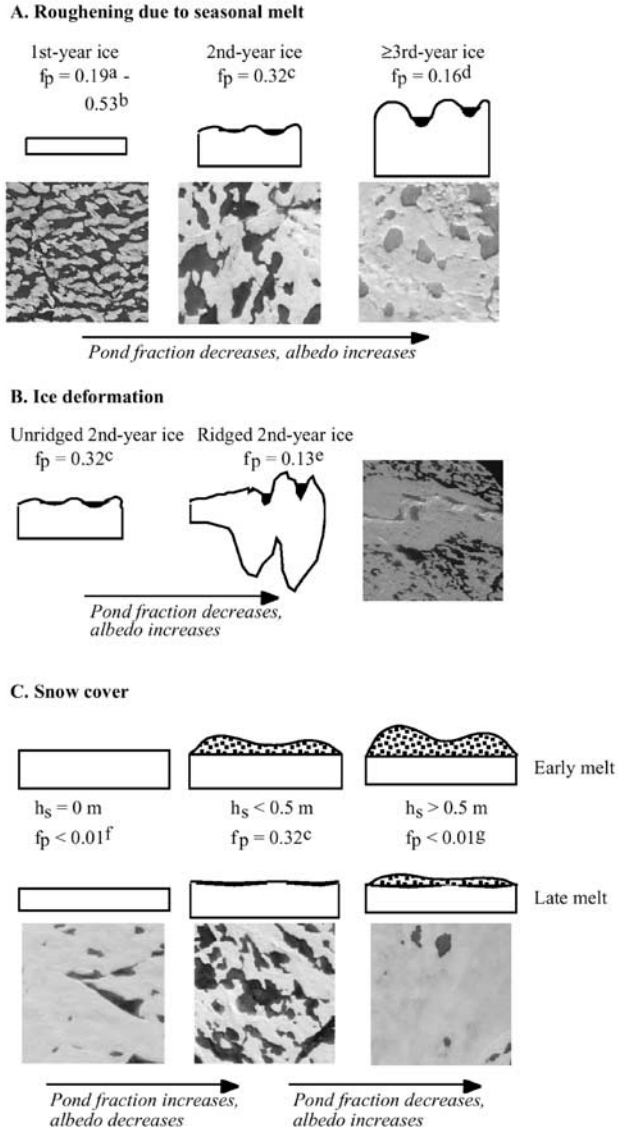

Figure 9. Schematic depiction of dependence of pond areal coverage on ice roughness (deformation and melt induced) and snow depth. Aerial photographs were obtained in the vicinity of SHEBA camp on 20 July and 7 August of 1998 and at Barrow on 22 June of 2001 (frames approximately 150 and 400 m across). Pond areal fractions are (f_p) based on different data sets. Footnotes given in the figure are as follows: a, Barrow 2001 (see Table 2); b, maximum observed in Canadian Arctic landfast ice [*Derksen et al.*, 1997]; c, SHEBA (see Table 2); d, Eurasian Arctic [*Eicken et al.*, 1994]; e, SHEBA ridged multiyear ice [*Eicken et al.*, 2001]; f, inferred from SHEBA Airport Lead data [*Eicken et al.*, 2002] and aerial photography; and g, inferred for SHEBA surface ablation rates (for details see text). See color version of this figure at back of this issue.

ice extent as well as a reduced residence time of ice in the Arctic Basin [*Rothrock et al.*, 2003] need to be taken into consideration as well. With pond fractions dropping and hence albedo increasing during the ageing process of multiyear ice, a reduction in mean Arctic sea-ice age should be associated with an overall decrease in large-scale pack-ice albedo. Further work is required to determine the relative importance of these different factors for variability and trends in ice albedo.

5.2. Snow Cover–Permeability Linkages

[26] The impact of permeability on pond fractions and albedo is equally complex, as illustrated in Figure 9. With substantial seasonal variations in bulk ice permeability by more than 2 orders of magnitude [*Eicken et al.*, 2002], the progression of surface ablation rates and timing of critical events such as the complete removal of the snow cover exposing the bare ice surface gain substantially in importance for the seasonal pond evolution. This sensitivity to changes in boundary conditions is greatly diminished during the second half of the melt season when pond water levels are close to hydrostatic equilibrium and melting has locked ponds into surface depressions (Figures 5, 8b, and 8d). In light of these constraints, snow accumulation on the sea ice needs to be considered as one of the most critical variables in determining ice permeability and hence pond areal fractions (Figure 9). This finding is underscored by the interannual contrasts in pond fraction observed at Barrow as well as by the aerial photographs of unridged ice shown in Figure 9. Typically, level first-year ice exhibits the highest pond fractions of any ice type [*Derksen et al.*, 1997; *Fetterer and Untersteiner*, 1998; *Hanesiak et al.*, 2001], yet, at SHEBA a substantial portion of the first-year ice cover, estimated at between 10 and 30%, exhibited low or zero pond coverage (Figure 9c). On the basis of indirect evidence (we are lacking direct field measurements in the footprint of the aerial photographs), we interpret the unponded ice to have formed on leads and open water in the winter, seeing little to no snow accumulation resulting in rapid ice growth and higher ice salinities. Such ice exhibits substantially higher permeabilities allowing for efficient drainage of surface meltwater. This interpretation is substantiated not only by the contrasts in ice permeability and superimposed ice formation found at Barrow in 2000 and 2001 (Table 2, Figures 6 and 5), but also by the large-scale experiment conducted at SHEBA through removal of snow from a frozen lead for maintenance of a sea-ice runway. This snow-free lead ice did not develop any melt ponds and lacked a superimposed ice layer that was ubiquitous at other snow-covered first-year and multiyear sites near the SHEBA camp [*Eicken et al.*, 2002]. While the survival of the runway ice very late into the summer season is in part also attributed to its greater thickness in comparison with lead ice formed in midwinter, the snow removal experiment nevertheless demonstrates the importance of the snow cover in controlling pond evolution and suggests the need for a more detailed assessment under natural conditions.

[27] At some point, an increase in snow depth can actually result in a suppression of pond coverage and a concurrent increase in ice albedo. This occurs when snow is not completely removed during the summer or complete melt-off is shifted into the latter part of the melt season. Research during the early phase of the summer at the SHEBA site in deeper snow has shown that under such conditions, meltwater builds up at the base of the snowpack but is not actually exposed in the form of low-albedo melt

ponds. For the snow ablation rates observed at SHEBA (3.5 ± 0.6 mm d^{-1} between 27 May and 24 June), incomplete removal of snow would at most have required a snow depth of 0.9 m. However, considering differences in snow and bare ice albedo and reductions in surface ablation during the second half of the melt season, a snow depth on the order of 0.5 m is probably a better representation of the critical threshold value. We are not aware of current locations in the Arctic proper where such a situation occurs on larger scales. At SHEBA, even the roughly 5% of snow depth gauges located at sites with snow depths above 0.9 m (0.97 m maximum) had lost all the snow cover by the second week of August. Nevertheless, at higher latitudes or during shorter summers, snow may well survive in some locations, as observed in the summer of 1996 in the Siberian Arctic [*Haas and Eicken*, 2001]. Similarly, observations of superimposed ice formation and general lack of melt ponds in the Antarctic [e.g., *Haas et al.*, 2001] and in sub-Arctic seas such as the Sea of Okhotsk [*Ukita et al.*, 2000] suggest that the snow may be deep enough (relative to the surface ablation rate) for this shielding effect to set in.

[28] A further, little documented process that may be of importance is the potential impact of rain events on pond evolution. Both at SHEBA and in Barrow, on a few occasions, rainfall was observed over the sea ice, adding to the surface meltwater input and presumably enhancing ablation rates. Total precipitation rates were not sufficient, however, to have a lasting impact on pond area and albedo, as the water supply from rain in most cases did not rival that of maximum daily surface ablation rates. Another important aspect relating to summer precipitation is whether it falls as rain or snow, since even a minor amount of snowfall can drive up surface albedo by as much as 10% at below-freezing temperatures. Such snowfall events are an important source of summer albedo variability [*Perovich et al.*, 2002a], and an increase in liquid rather than solid precipitation would significantly impact the sea-ice summer radiation balance.

5.3. Improving Albedo Parameterizations in Large-Scale Sea-Ice and Climate Models

[29] It is presently not at all clear how the different processes discussed above combine in controlling the surface albedo evolution of the ice pack under variable boundary conditions. It is clear, however, that GCMs are currently not well equipped to address these issues in an effective manner. This not only applies to the lack of process-based parameterizations of ice albedo but also extends to the simple fact that albedos of first-year ice can be substantially different from those of multiyear ice, a fact that is currently not captured in major GCMs [*Weatherly et al.*, 1998] (see also B. P. Briegleb et al., Description of the Community Climate System Model 2.0 Sea Ice Model, available online at www.ccsm.ucar.edu/models/ccsm2.0/csim/, 2002). The development of a full ice hydrology/albedo model based on the approach outlined here is beyond the scope of this paper. However, to assess the overall validity of the approach and gain further insight into the type of measurements and modeling required, we have performed a very crude simulation. For the second half of June 1998, we have compared albedo measurements at SHEBA with the albedo predictions obtained from the parameterization employed in the Geophysical Fluid Dynamics Laboratory (GFDL) global climate model [*Manabe et al.*, 1992], as shown in Figure 10. The GFDL albedo parameterization is given by

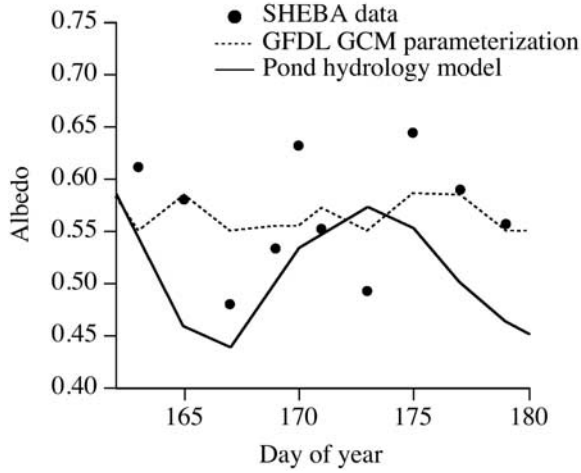

Figure 10. Surface albedo of level multiyear ice at the SHEBA site between 12 and 28 June in 1998. Shown are mean values from measurements along a 200-m profile as well as the parameterization employed in the GFDL GCM [*Manabe et al.*, 1992] and results from a crude pond hydrology-albedo model.

$$\begin{aligned} \alpha^* &= \alpha_i && T_s \geq T_m, \\ &= \alpha_i + 0.025(T_m - T_s) && (T_m - 10) < T_s < T_m, \\ &= \alpha_s && T_s \leq (T_m - 10), \\ \alpha_i &= 0.55 && \alpha_s = 0.8, \end{aligned} \tag{7}$$

where α^* is the total albedo, which is assumed to correspond to the bare ice albedo α_i (which includes a constant pond fraction) at surface (air) temperature T_s above or equal to the ice melting temperature T_m (0°C) and exhibits a linear increase to values corresponding to the snow albedo α_s at temperatures equal to or less than 10 K below the surface melting temperature. Air temperatures have been obtained from the SHEBA surface meteorology data set [*Perovich et al.*, 1999]. With the surface temperature varying within comparatively small bounds, the parameterization does not capture the substantial variations in surface albedo (Figure 10). In order to arrive at an estimate of surface albedo based on the pond hydrological model for an ice permeability of 10^{-12} m^2 and 2.5 m ice thickness (equation (5)), pond areal coverage has been computed based on surface ablation rates (measured at 2-day intervals [*Perovich et al.*, 2003]) and the surface topography of level multiyear ice (Figure 8). Albedo α was then derived from the pond areal fraction f_p based on the data set of measured albedos and pond fractions estimated within the instrument footprint (as shown for first-year ice in Figure 1).

[30] Despite the various shortcomings and errors involved in this approach (surface topography does not evolve with

time, constant permeability, assumption of steady state, coarse temporal resolution and high short-term error in surface ablation measurements, etc.), the resulting albedo time series does exhibit a range comparable to that of the measured data. The overall sequence of low- and high-albedo phases also agrees reasonably well with the measurements when taking into account that the model does not reproduce the much higher short-term variations in surface melt rate and assumes instantaneous dispersal and relaxation to steady state. Apart from a more sophisticated hydrological model, an in-depth validation would require ice surface ablation data collected at much higher temporal resolution than is currently the case with standard mass balance gauges [*Perovich et al.*, 2003]. Thus the offset between measured albedo and the pond hydrologic model (Figure 10) is in part due to the fact that surface ablation was only measured every 2 days (often out of phase with albedo measurements), such that the timing of melt episodes and corresponding albedo changes was off by a day or two. A thermodynamic sea-ice model may be more successful in providing ablation rates for such short time steps, and the standard albedo parameterization actually gets the timing (though not the amplitude) of some of these events right because it is directly tied to temperature rather than measured ablation rate. A further requirement would be better data or model simulations of the evolution of the surface topography as a function of time. Given that the ice surface can change substantially over timescales of days to weeks (Figures 5 and 8) and considering the importance of topography in steering meltwater flow and retention, this may require more substantial field and modeling efforts in the future.

6. Conclusions

[31] The seasonal evolution of Arctic sea ice albedo is strongly dependent on melt pond coverage, f_p, which in turn depends critically on ice surface ablation rates, topography, and permeability. During early melt, pond level variations translate directly into substantial changes in f_p and albedo at short timescales. Reductions in hydraulic head and steepening pond margins greatly reduce this sensitivity. Early melt can hence control later ice albedo evolution. The present study suggests that the surface elevation of melt ponds varies by <0.2 m, and differences of a few centimeters can double the pond fraction f_p, exceeding the capabilities of presently available GCMs and ice models to predict summer ice albedo. While model parameterizations [e.g., *Weatherly et al.*, 1998; *Curry et al.*, 2001] are not likely to capture the substantial short-term and interannual variability of albedo, the magnitude and exact nature of potential discrepancies needs to be investigated. Hydrological modeling indicates, however, that such problems can be circumvented by large-scale, high-resolution measurements of ice-surface topography, for example, through airborne laser altimeters. An approach integrating the topographic statistics of different ice types and ages rather than point-by-point measurements may already suffice. On the basis of such data sets, which to our knowledge are not yet available, one could then assign or assimilate different topographic statistics for the various relevant age classes and types of sea ice that can be represented in a specific model. While this does not yet yield a fully independent, physically based prediction, the approach taken here is a first and possibly key step in improving the representation of ice albedo in sea-ice and climate models based on the underlying physical processes rather than potentially inadequate parameterizations. Ultimately, hydrological modeling could be combined with a fully coupled radiative transfer-ice growth model to allow the ice topography and meltwater fluxes as well as pond and ice optics to evolve independently.

[32] While more detailed studies need to gauge the relative importance of topography versus snow effects on permeability, the former appears to dominate the spatial variability and seasonal evolution of pond coverage. Snow cover, however, can strongly affect interannual variability in ponding over the Arctic Basin. Given the large interannual variability of moisture fluxes and precipitation in the Arctic [*Overland et al.*, 1996] combined with the effects of climate change [*Folland et al.*, 2001], superimposed ice and ponding can substantially complicate predictions of the surface radiation balance. As a result of decreased summer minimum ice extent in the Arctic [*Comiso*, 2002], the amount of first-year sea ice has increased substantially in the past decade. Given the wide range of pond fractions and albedos observed over first-year ice and considering furthermore that first-year ice albedos differ substantially from those of multiyear ice, which are currently defining albedo parameterizations in GCMs [*Weatherly et al.*, 1998] (see also B. P. Briegleb et al., Description of the Community Climate System Model 2.0 Sea Ice Model, available online at www.ccsm.ucar.edu/models/ccsm2.0/csim/, 2002), we recognize a definite need for both field and model investigations leading to improved representation of ice albedo in large-scale simulations of the changing Arctic ice pack.

[33] **Acknowledgments.** Support from the National Science Foundation (OPP-9872573 and 9910888) and the Office of Naval Research is gratefully acknowledged. The Atmospheric Radiation Program (ARM) and NOAA Climate Monitoring and Diagnostics Laboratory provided shortwave radiation data. We thank Nori Tanaka and Gordon Bower for stable-isotope measurements. Barrow Arctic Science Consortium, CGC *Des Groseilliers* crew, M. Sturm, K. Liggett, M. Gould, J. Freitag, S. Chang, D. Cole, and L. Shapiro provided valuable help and comments. Thanks also go to T. George for excellent flight support. The comments by J. Walsh, G. Maykut, N. Untersteiner, R. Kwok, and two anonymous reviewers helped to significantly improve the manuscript.

References

Cherepanov, N. V. (1973), Main results of an investigation of the crystal structure of sea ice, *Probl. Arct. Antarct., Engl. Transl.*, *41*, 43–54.

Comiso, J. C. (2002), A rapidly declining perennial sea ice cover in the Arctic, *Geophys. Res. Lett.*, *29*(20), 1956, doi:10.1029/2002GL015650.

Covey, C., K. E. Taylor, and R. E. Dickinson (1991), Upper limit for sea ice albedo feedback contribution to global warming, *J. Geophys. Res.*, *96*(D5), 9169–9174.

Cox, G. F. N., and W. F. Weeks (1983), Equations for determining the gas and brine volumes in sea-ice samples, *J. Glaciol.*, *29*, 306–316.

Curry, J. A., J. L. Schramm, and E. E. Ebert (1995), Sea ice-albedo climate feedback mechanism, *J. Clim.*, *8*, 240–247.

Curry, J. A., J. L. Schramm, D. K. Perovich, and J. O. Pinto (2001), Applications of SHEBA/FIRE data to evaluation of snow/ice albedo parameterizations, *J. Geophys. Res.*, *106*(D14), 15,345–15,355.

Derksen, C., J. Piwowar, and E. LeDrew (1997), Sea-ice melt-pond fraction as determined from low level aerial photographs, *Arct. Alp. Res.*, *29*, 345–351.

Eicken, H., R. Gradinger, B. Ivanov, A. Makshtas, and R. Pác (1994), Surface melt puddles on multi-year sea ice in the Eurasian Arctic, in *World Climate Research Programme WCRP-94: Proceedings of the ACSYS Conference on the Dynamics of the Arctic Climate System*

(Göteborg, Sweden, 7–10 November 1994), *WMO/TD 760*, pp. 267–271, World Meteorol. Org., Geneva.

Eicken, H., W. B. Tucker III, and D. K. Perovich (2001), Indirect measurements of the mass balance of summer Arctic sea ice with an electromagnetic induction technique, *Ann. Glaciol.*, *33*, 194–200.

Eicken, H., H. R. Krouse, D. Kadko, and D. K. Perovich (2002), Tracer studies of pathways and rates of meltwater transport through Arctic summer sea ice, *J. Geophys. Res.*, *107*(C10), 8046, doi:10.1029/2000JC000583.

Eicken, H., D. M. Cole, and L. H. Shapiro (2004), Permeability-porosity relationships in first-year Arctic sea ice, in preparation.

El Naggar, S., C. Garrity, and R. O. Ramseier (1998), The modelling of sea ice melt-water ponds for the High Arctic using an airborne line-scan camera, and applied to the Satellite Special Sensor Microwave/Imager (SSM/I), *Int. J. Remote Sens.*, *19*, 2373–2394.

Fetterer, F., and N. Untersteiner (1998), Observations of melt ponds on Arctic sea ice, *J. Geophys. Res.*, *103*(C11), 24,821–24,835.

Folland, C. K., T. R. Karl, J. R. Christy, R. A. Clarke, G. V. Gruza, J. Jouzel, M. E. Mann, J. Oerlemans, M. J. Salinger, and S.-W. Wang (2001), Observed climate variability and change, in *Climate Change 2001, The Scientific Basis: Contribution of Working Group I to the Third Assessment Report of the Intergovernmental Panel on Climate Change*, edited by J. T. Houghton et al., pp. 99–181, Cambridge Univ. Press, New York.

Freitag, J. (1999), The hydraulic properties of Arctic sea ice: Implications for the small-scale particle transport (in German), *Ber. Polarforsch.*, *325*, 150 pp.

Freitag, J., and H. Eicken (2003), Melt water circulation and permeability of Arctic summer sea ice derived from hydrological field experiments, *J. Glaciol.*, *49*, 349–358.

Frey, K., H. Eicken, D. K. Perovich, T. C. Grenfell, B. Light, L. H. Shapiro, and A. P. Stierle (2001), Heat budget and decay of clean and sediment-laden sea ice off the northern coast of Alaska, paper presented at Port and Ocean Engineering in the Arctic Conference (POAC'01), Port and Ocean Eng. Under Arctic Cond., Ottawa.

Grenfell, T. C., and D. K. Perovich (1984), Spectral albedos of sea ice and incident solar irradiance in the southern Beaufort Sea, *J. Geophys. Res.*, *89*(C3), 3573–3580.

Haas, C., and H. Eicken (2001), Interannual variability of summer sea ice thickness in the Siberian and Central Arctic under different atmospheric circulation regimes, *J. Geophys. Res.*, *106*(C3), 4449–4462.

Haas, C., D. N. Thomas, and J. Bareiss (2001), Surface properties and processes of perennial Antarctic sea ice in summer, *J. Glaciol.*, *47*, 613–625.

Hanesiak, J. M., D. G. Barber, R. De Abreu, and J. J. Yackel (2001), Local and regional albedo: Observations of Arctic first-year sea ice during melt ponding, *J. Geophys. Res.*, *106*(C1), 1005–1016.

Hanson, A. M. (1965), Studies of the mass budget of Arctic pack-ice floes, *J. Glaciol.*, *5*, 701–709.

Lemke, P., W. D. Hibler, G. Flato, M. Harder, and M. Kreyscher (1997), On the improvement of sea-ice models for climate simulations: The Sea Ice Model Intercomparison Project, *Ann. Glaciol.*, *25*, 183–187.

Leppäranta, M., and T. Manninen (1988), The brine and gas content of sea ice with attention to low salinities and high temperatures, *Internal Rep. 88-2*, Finn. Inst. of Mar. Res., Helsinki.

Manabe, S., M. J. Spelman, and R. J. Stouffer (1992), Transient responses of a coupled ocean-atmosphere model to gradual changes of atmospheric CO_2: II. Seasonal response, *J. Clim.*, *5*, 105–126.

Maykut, G. A. (1986), The surface heat and mass balance, in *The Geophysics of Sea Ice*, edited by N. Untersteiner, pp. 395–463, Martinus Nijhoff, Zoetermeer, Netherlands.

Overland, J. E., P. Turet, and A. H. Oort (1996), Regional variations of moist static energy flux into the Arctic, *J. Clim.*, *9*, 54–65.

Parry, W. E. (1828), *Narrative of an Attempt to Reach the North Pole, in Boats Fitted for the Purpose, and Attached to His Majesty's Ship Hecla, in the Year MDCCCXXVII, Under the Command of Captain William Edward Parry*, J. Murray, London.

Pegau, W. S., and C. A. Paulson (2001), The albedo of Arctic leads in summer, *Ann. Glaciol.*, *33*, 221–224.

Perovich, D. K., et al. (1999), Year on ice gives climate insights, *Eos Trans. AGU*, *80*(481), 485–486.

Perovich, D. K., T. C. Grenfell, B. Light, and P. V. Hobbs (2002a), Seasonal evolution of the albedo of multiyear Arctic sea ice, *J. Geophys. Res.*, *107*(C10), 8044, doi:10.1029/2000JC000438.

Perovich, D. K., W. B. Tucker III, and K. A. Ligett (2002b), Aerial observations of the evolution of ice surface conditions during summer, *J. Geophys. Res.*, *107*(C10), 8048, doi:10.1029/2000JC000449.

Perovich, D. K., T. C. Grenfell, J. A. Richter-Menge, B. Light, W. B. Tucker III, and H. Eicken (2003), Thin and thinner: Sea ice mass balance measurements during SHEBA, *J. Geophys. Res.*, *108*(C3), 8050, doi:10.1029/2001JC001079.

Robinson, D. A., M. C. Serreze, R. G. Barry, G. R. Scharfen, and G. Kukla (1992), Large-scale patterns and variability of snowmelt and parameterized surface albedo in the Arctic Basin, *J. Clim.*, *5*, 1109–1119.

Romanov, I. P. (1995), *Atlas of Ice and Snow of the Arctic Basin and Siberian Shelf Seas*, 2nd ed., Backbone, New York.

Rothrock, D. A., J. Zhang, and Y. Yu (2003), The arctic ice thickness anomaly of the 1990s: A consistent view from observations and models, *J. Geophys. Res.*, *108*(C3), 3083, doi:10.1029/2001JC001208.

Schramm, J. L., M. M. Holland, J. A. Curry, and E. E. Ebert (1997), Modeling the thermodynamics of a sea ice thickness distribution: 1. Sensitivity to ice thickness resolution, *J. Geophys. Res.*, *102*(C10), 23,079–23,091.

Serreze, M. C., J. E. Walsh, F. S. Chapin III, T. Osterkamp, M. Dyurgerov, V. Romanovsky, W. C. Oechel, J. Morison, T. Zhang, and R. G. Barry (2000), Observational evidence of recent change in the northern high-latitude environment, *Clim. Change*, *46*, 159–207.

Shapiro, L. H., and P. W. Barnes (1991), Correlation of nearshore ice movement with seabed ice gouges near Barrow, Alaska, *J. Geophys. Res.*, *96*(C9), 16,979–16,989.

Steele, M., and G. M. Flato (2000), Sea ice growth, melt, and modeling: A survey, in *The Freshwater Budget of the Arctic Ocean*, edited by E. L. Lewis, pp. 549–587, Kluwer Acad., Norwell, Mass.

Tschudi, M. A., J. A. Curry, and J. A. Maslanik (2001), Airborne observations of summertime surface features and their effect on surface albedo during FIRE/SHEBA, *J. Geophys. Res.*, *106*(D14), 15,335–15,344.

Ukita, J., T. Kawamura, N. Tanaka, T. Toyota, and M. Wakatsuchi (2000), Physical and stable isotopic properties and growth processes of sea ice collected in the southern Sea of Okhotsk, *J. Geophys. Res.*, *105*(C9), 22,083–22,093.

Untersteiner, N. (1990), Structure and dynamics of the Arctic Ocean ice cover, in *The Arctic Ocean Region*, edited by A. Grantz, L. Johnson, and J. F. Sweeney, pp. 37–51, Geol. Soc. of Am., Boulder, Colo.

Walsh, J. E., J. Curry, M. Fahnestock, M. C. Kennicutt II, A. D. McGuire, W. B. Rossow, M. Steele, C. J. Vorosmarty, and R. Wharton (2001), *Enhancing NASA's Contribution to Polar Science: A Review of Polar Geophysical Data Sets*, Natl. Acad., Washington, D. C.

Weatherly, J. W., B. P. Briegleb, W. G. Large, and J. A. Maslanik (1998), Sea ice and polar climate in the NCAR CSM, *J. Clim.*, *11*, 1472–1486.

Yackel, J. J., and D. G. Barber (2000), Melt ponds on sea ice in the Canadian Archipelago: 2. On the use of RADARSAT-1 synthetic aperture radar for geophysical inversion, *J. Geophys. Res.*, *105*(C9), 22,061–22,070.

H. Eicken, Geophysical Institute, University of Alaska Fairbanks, Fairbanks, AK 99775-7320, USA. (hajo.eicken@gi.alaska.edu)

T. C. Grenfell, Department of Atmospheric Sciences, University of Washington, Seattle, WA 98195-1640, USA. (tcg@atmos.washington.edu)

D. K. Perovich and J. A. Richter-Menge, Cold Regions Research and Engineering Laboratory, Hanover, NH 03755-1290, USA. (perovich@crrel.usace.army.mil; jrichtermenge@crrel41.crrel.usace.army.mil)

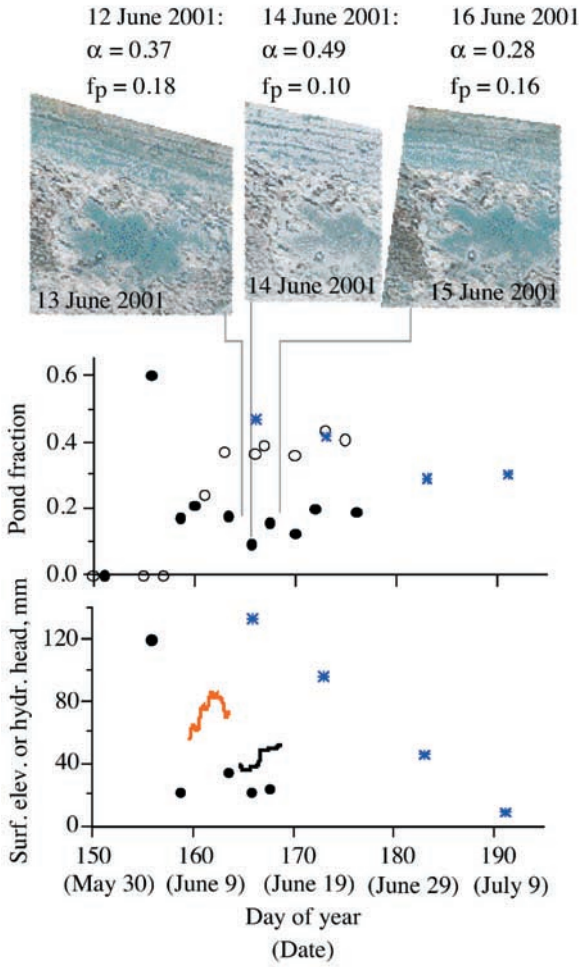

Figure 3. Areal fraction and hydraulic head of melt ponds in multiyear ice (asterisks, measurements carried out at SHEBA sites along a 100-m profile through level ice) and first-year ice near Barrow (open circles: 2000; dots: 2001). Solid lines show water level in a single pond (pressure-gauge measurement; red: 2000; black: 2001). Aerial photographs (top middle panel, ~600 m wide; dates of overflights indicated at bottom of photograph) show a sequence of drainage and flooding events in first-year ice near Barrow. Also shown are areally averaged albedo α and pond fraction f_p (measurement dates are indicated at top; note that on two dates, synchronous overflights and ground-based measurements were not possible).

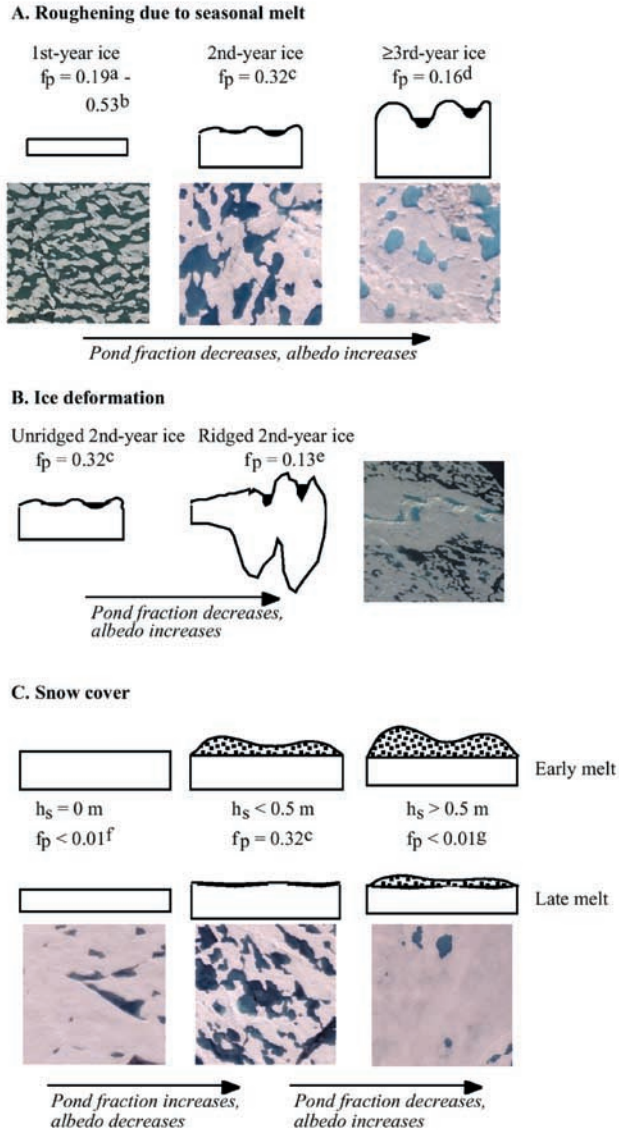

Figure 9. Schematic depiction of dependence of pond areal coverage on ice roughness (deformation and melt induced) and snow depth. Aerial photographs were obtained in the vicinity of SHEBA camp on 20 July and 7 August of 1998 and at Barrow on 22 June of 2001 (frames approximately 150 and 400 m across). Pond areal fractions are (f_p) based on different data sets. Footnotes given in the figure are as follows: a, Barrow 2001 (see Table 2); b, maximum observed in Canadian Arctic landfast ice [*Derksen et al.*, 1997]; c, SHEBA (see Table 2); d, Eurasian Arctic [*Eicken et al.*, 1994]; e, SHEBA ridged multiyear ice [*Eicken et al.*, 2001]; f, inferred from SHEBA Airport Lead data [*Eicken et al.*, 2002] and aerial photography; and g, inferred for SHEBA surface ablation rates (for details see text).